Technical note: implications of using EGSnrc instead of EGS4 for extracting electron stopping powers from measured energy spectra

Tessier, Frédéric; Ross, Carl K.

Publisher's version / Version de l'éditeur:
https://doi.org/10.1002/mp.14567
Medical Physics, pp. 1-9, 2020-10-30

Technical Note: Implications of using EGSnrc instead of EGS4 for extracting electron stopping powers from measured energy spectra

Frédéric Tessier[1] and Carl Kenneth Ross[2]

Ionizing Radiation Standards, Metrology Research Centre,
National Research Council Canada, Ottawa, Ontario K1A 0R6 Canada

[1]Corresponding author: Frederic.Tessier@nrc-cnrc.gc.ca
[2]Retired

November 16, 2020

Abstract

Purpose NRC Report PIRS 0626 (https://doi.org/10.4224/40000364) describes how measured electron energy deposition spectra can be used to determine the electronic stopping power. The stopping power is obtained by comparing measured spectra with spectra calculated using Monte Carlo techniques. The stopping powers reported in PIRS 0626 were obtained using the EGS4 Monte Carlo code. Since then, the EGSnrc code has been released which has more accurate electron transport algorithms. We calculate the effect on the measured stopping powers of using EGSnrc instead of EGS4.

Method The EGS4 spectra calculated in PIRS 0626 were based on 4×10^5 primary electron histories. We first show that those spectra, calculated in 1997, are consistent with current EGS4 spectra calculated using 10^8 histories. EGSnrc spectra are also calculated using 10^8 histories and these high-precision spectra are compared to extract any energy difference. The energy differences between the spectra are used to estimate the effect on the measured electronic stopping powers.

Results The energy differences depend on the absorber material, the absorber thickness and the beam energy. The improved electron elastic scattering cross section of EGSnrc accounts for only part of the difference between the two codes. The effect on the extracted stopping power is largest for the lowest electron energies and can be as large as 0.9 %. The calculated spectra show differences for lower energies, with the EGSnrc spectra having a larger proportion of low energy electrons.

Conclusion The differences introduced by using EGSnrc instead of EGS4 can affect the estimated stopping power by almost 1 % in the worst case but generally the effect is much smaller. We report corrections that can be applied to all the stopping power data in PIRS-0626. An experiment to measure the average energy to create an ion pair in air, W_{air}, using

aluminum detectors will provide an interesting test of the aluminum stopping power data as reported in PIRS 0626 and revised by this work.

keywords: EGS4, EGSnrc, electronic stopping powers, electron energy spectra, NaI detector, energy to create an ion pair

running title: Stopping powers with EGSnrc vs EGS4

1 Introduction

As noted in ICRU Report 90[1], electron stopping powers are key data for radiation dosimetry and radiation metrology. In particular, the electronic[1] component of the stopping power is one of the main inputs for dosimetry protocols[2,3] based on either air kerma or absorbed dose standards. It is also critical for the accuracy of Monte Carlo (MC) codes[4,5] because it defines the energy loss in inelastic collisions.

Despite its importance, there are very few measurements of the electron electronic stopping power. Instead, the best estimates are based on a theoretical model[6], combined with empirical data for the mean excitation energy, I. These stopping powers are estimated to have a standard uncertainty of 0.5 % to 1 % for electron energies greater than about 1 MeV and have been tabulated for a wide range of materials in ICRU Report 37[6]. The uncertainty can be somewhat larger for granular materials where there is ambiguity as to what density to use when evaluating the density effect. In the case of graphite, which is widely used for radiation dosimetry, using the bulk versus the grain density can change the electronic stopping power by about 1 %.

ICRU Report 37 compares measured and calculated stopping powers. Electronic stopping powers have been measured for electron energies below about 130 keV, but the report concludes that "...the differences between theory and experiment do not form a consistent pattern ...". Two sets of measurements are reported for the total stopping power in the energy range from about 3 MeV to 30 MeV, but the uncertainties are typically greater than 5 %. Thus, at the time when ICRU Report 37 was prepared, there were no measurements of the electronic stopping power in the energy range of importance to radiation therapy that could serve as a definitive test of the tabulated values.

In an effort to test the stopping power data tabulated in ICRU 37, the National Research Council of Canada (NRC) embarked on a program[7] to directly measure the electronic stopping power. The basic idea was to measure the electron energy deposition spectrum of a monoenergetic electron beam after passing through an absorbing slab with well-defined properties and compare it to the same spectrum calculated using some MC code. Any energy

[1] Often referred to as the collision stopping power, the ICRU now recommends electronic stopping power.

shift between the two spectra would be identified as an error in the stopping power used for the MC calculation.

The details of the procedure and the results obtained are available in an NRC report[8] so only a brief outline will be repeated here. The detector system used for the measurements is shown in Figure 1 and consisted of a large NaI detector[2] that was used to measure the energy deposition spectrum, with and without, an absorbing slab in place. The full geometry was originally modelled using the EGS4[10] MC code. While reviewing the geometry input to generate Figure 1, we noted that part of the lateral aluminum mount and lead shielding was missing in the original model (revealed as a full radius air gap above the detector). We verified that the distance between the absorber and the detector was correct, and that the calculated spectra are not sensitive to this lack of lateral shielding (data not shown). Figure 2 shows a spectrum measured using 15 MeV electrons and a 2 g cm^{-2} Al absorber. The dashed line shows, in principle, what the calculated MC spectrum might look like, but the energy offset has been exaggerated to illustrate the technique. In this example, the calculated energy loss in the absorber is less by ϵ than the measured energy loss, thus indicating that the stopping power for 15 MeV electrons used by the MC code is too small.

In principle, the stopping power could be modified slightly and the MC calculation repeated to generate a new offset. This iterative procedure could be repeated until ϵ is close to zero. Because of the large number of MC calculations required this approach is not practical and instead, a correction to the stopping power is estimated using the measured value of ϵ. ICRU Report 35[11] states that the approximate change in the most probable energy after an electron passes through an absorber is given by the product of the absorber thickness and the electronic stopping power. PIRS-0626 modified this relationship to allow for path length straggling as

$$\kappa = \frac{\epsilon}{t_{\mathrm{pl}}}, \tag{1}$$

where κ is a correction to the electronic stopping power and t_{pl} is the electron path length through an absorber with thickness t_{slab}. (In PIRS-0626, t_{pl} was denoted by $t^{\mathrm{r}}_{\mathrm{eff}}$). The fitting procedure to extract ϵ is most sensitive to electron energies near the high-energy inflection point of the spectrum. Thus, t_{pl} is the path length appropriate for those electrons. t_{pl} is expected to be close to, but larger than, t_{slab} because of path length straggling.

[2] There has been a recent proposal[9] to use a Ge detector.

Eq. 1 should be an accurate estimate of the stopping power correction if κ is small. If one were to encounter a situation where κ is a significant fraction of the stopping power then the MC calculation should be repeated with the revised stopping power and a new value of κ obtained.

Note that ϵ is taken to be positive when the MC spectrum lies to the right of the measured spectrum and negative when it lies to the left. A positive value of ϵ implies that the stopping power is too low.

Major improvements to the EGS4 code led to the introduction of EGSnrc[4,12,13] after the work in PIRS 0626 was completed. Some of the changes involved electron transport and might affect the calculated electron spectra that were used to estimate the corrections to the electron stopping power. In particular, electron elastic cross sections including relativistic spin effects were introduced. The objective of this work is to compare electron spectra calculated with EGS4 and EGSnrc, extract any energy shifts between the spectra and use these shifts to correct the stopping power data presented in PIRS 0626.

2 Materials and Methods

We had access to the original EGS4 spectra which were calculated using the `DOSRZ` application and 4×10^5 primary electron histories. In order to compare calculated spectra that were largely free of statistical errors we wished to compute spectra using 10^8 histories. We first demonstrated that high-precision spectra calculated using the version of `DOSRZ` used in 1997 agreed with the original spectra. To this end, a copy of the legacy DOSRZ Fortran source code (last edited in February 1998) was recovered and adjusted slightly to curb compiler errors for system calls, and to match the format of the available input files and output spectra. Note that the same physical data was used for the high-precision calculations. In particular, the stopping data was that of ICRU Report 37, with the crystalline density used to evaluate the density effect of graphite. To verify that our high-precision EGS4 spectra were consistent with those calculated in 1997, we fitted one to the other to extract the energy shift (see Supplementary Material Figure S-1 and Figure S-2).

The input files used by DOSRZ were then converted to the format required by the EGSnrc application, DOSRZnrc[14], using morph_dosrz[3] and a custom python script. Simulation parameters were left unchanged compared to the EGS4 version, except for the addition of the following EGSnrc specific ones: a) bound Compton scattering was set to "off"; b) spin effects were turned "on"; 3) the bremsstrahlung cross section was set to "NRC"; and 4) the electron transport algorithm was set to "EGSnrc", with "Exact" boundary-crossing (defaults in EGSnrc). Spectra were generated using 10^8 incident electrons and 10 keV energy bins. The physical data (the same pegs4 file) was the same as that for the EGS4 calculations. A sample EGSnrc input file specifying the detector geometry is provided as Supplementary Material file dosrz-10al10.egsinp.

Each EGSnrc spectrum was fitted to the corresponding EGS4 spectrum by minimizing χ^2 defined by

$$\chi^2 = \sum_{i=L}^{H} \frac{(y_\mathrm{r}(E_i) - s y_\mathrm{f}(E_i + \Delta E))^2}{u_{\mathrm{c,r}}(E_i)^2 + s^2 u_{\mathrm{c,f}}(E_i + \Delta E)^2}, \tag{2}$$

where $y_\mathrm{r}(E_i)$ is the reference spectrum (EGS4) and $y_\mathrm{f}(E_i)$ is the spectrum to be fitted (EGSnrc). The corresponding standard uncertainties are $u_{\mathrm{c,r}}(E_i)$ and $u_{\mathrm{c,f}}(E_i)$. The fitting parameters consisted of a scale factor, s, and an energy shift, ΔE, and these were obtained by minimizing χ^2 using RStudio[15]. Values of $y_\mathrm{f}(E_i + \Delta E)$ and $u_{\mathrm{c,f}}(E_i + \Delta E)$ were obtained from linear interpolation between adjacent bins. The fitting range encompassed the peak of the spectrum, from 80 % of the peak value on the low-energy side to 5 % of the peak value on the high-energy side. The summation limits, L and H, are the bin numbers corresponding to these energy limits. The scale factor is mainly determined by the spectral peak while the energy shift is most sensitive to the spectra near the high-energy inflection point. The uncertainties of s and ΔE were obtained[16] by determining their values that gave $\chi^2_{\mathrm{min}} + 1$, where χ^2_{min} is the minimum value of χ^2. When fitting low-precision spectra, χ^2 may show structure near the minimum as ΔE crosses energy bins. In these cases, χ^2 was fitted to a parabola near its minimum and ΔE and its uncertainty determined from the properties of the parabola.

Nominal electron beam energies were 5, 7, 10, 15, 20, 25 and 30 MeV, although only a few measurements were carried out at 5 MeV. Five elemental materials (beryllium, graphite, aluminum, copper and tantalum) were used, along with one compound (water) and two mix-

[3]in-house program written by A Merovitz and DWO Rogers, 1998

tures (A-150 tissue-equivalent plastic and C-552 air-equivalent plastic). Nominal thicknesses of the absorbing slabs varied from 0.25 to 4 g cm^{-2}, depending on the beam energy.

Eq. 1 can be rewritten as

$$\kappa' = \frac{\epsilon'}{t_{\mathrm{pl}}}, \tag{3}$$

where the prime notation is used to indicate that it is only the energy shift between the EGSnrc and EGS4 spectra that is being considered. In subsequent graphs, κ' is expressed as a percentage of the electronic stopping power. MacPherson[8] estimated t_{pl} by considering only the path lengths of electrons with an exit angle smaller than 20°. A more consistent approach is to record the electron path length inside the absorber as a function of the energy deposited in the detector, and consider only those electrons that contribute to the fitting procedure. Because of path length straggling, there will be a distribution of path lengths associated with each energy. To this end, during the EGSnrc simulation, we tally the average path length and its standard deviation as a function of deposited energy.

3 Results

We first demonstrated that the MC spectra used for the 1997 analysis are consistent with those calculated for this work using EGS4 and 10^8 primary histories. To do so, we calculated the energy shift, ΔE between the low- and high-precision spectra. Values of ΔE are statistically consistent with zero, with 78 % of the values lie within one standard deviation of zero, confirming that we are able to reproduce the results from 1997 but with higher precision.

Fitting the high-precision EGSnrc spectra to the corresponding EGS4 spectra gave the energy shifts shown in Figure 3 and Figure 4. The reduced χ^2 for the fits ranged from 0.5 to 20, with the largest values occurring for the Ta absorbers. The statistical uncertainties of the energy shifts are typically less than 0.1 keV but can be as large as 0.2 keV. Note that the EGS4 spectra, because they are the basis of the analysis of PIRS-0626, were taken as the reference spectra. A positive energy shift means that the EGSnrc spectrum is shifted to higher energy. If this difference were to be assigned to the stopping power, then the stopping power would need to increase in order to match the energy loss predicted by EGS4.

As stated in Section 2, t_{pl} was determined by calculating the electron path length through the slab as a function of the energy deposited in the detector. Figure 5 shows the result obtained for 10 MeV electrons incident on a slab of aluminum 0.3033 cm thick. The path length, averaged over the fitting range, is about 2.5 % greater than the slab thickness. Table 1 summarizes the results for different materials and energies. For a given deposited energy exiting the slab, there is a distribution of path lengths but Table 1 shows that the standard deviation of the distribution is at most 15 % in the highest scattering scenario (low energy in a high-Z material). If the distribution were much broader, it might call into question the validity of using a mean value for t_{pl}. We also report the typical number of MC multiple-scattering electron steps taken to cross the slab to demonstrate that t_{pl} is not based on only a few multiple scattering steps.

The largest difference between the electron path length and the slab thickness occurs for low-energy electrons passing through high-Z material. In the case of 7 MeV electrons and Ta, the difference is about 14 % but is generally much smaller. It will be shown that the contribution of κ' to the electronic stopping power is always less than 1 %, which means that using t_{pl} rather than t_{slab} will change the contribution by about 0.15 %, in the worst case. Thus, for this work, we have approximated t_{pl} by t_{slab}.

Figure 6 and Figure 7 show how the energy shifts between the EGS4 and EGSnrc spectra affect the stopping power data reported in PIRS-0626. The data were calculated using Eq. 3 and are presented as a percentage of the electronic stopping power tabulated in ICRU Report 37.

One might suppose that the scatter in the data presented in Figure 6 and Figure 7 is due to the uncertainty arising from the fitting procedure. This is not the case, because the uncertainty in each datum is typically smaller than the size of the symbol. Instead, the scatter arises because we are assigning any difference between the EGS4 and EGSnrc spectra to the electronic stopping power whereas the difference is really due to changes in the MC transport algorithms. Assuming that EGSnrc is a more accurate model than EGS4, Figure 6 and Figure 7 show, on a point by point basis, how stopping power data extracted using EGS4 need to be adjusted.

Although EGSnrc is based on EGS4 it incorporates many improvements[4,12,13]. Some of the enhancements are only important for low energies but others improve the transport of high energy electrons. Perhaps one of the most important is the inclusion of relativistic spin effects in the multiple scattering theory. EGSnrc includes an option to turn off the spin correction and we have re-calculated the energy shifts by comparing the full EGSnrc model with EGSnrc/spin-off and the results are shown in Figure 8 and Figure 9. If the spin correction were the dominant effect we would expect the EGSnrc/spin-off simulations to be similar to EGS4 and thus Figure 8 and Figure 9 should be similar to Figure 3 and Figure 4. Instead, we see a trend, whereby the spin effect accounts for most of the energy shift for low and high values of Z but is negligible for intermediate values. This is qualitatively similar to the result reported by Kawrakow[13] whereby the range is larger for low Z and smaller for high Z.

Kawrakow[17] has given a detailed analysis of how each of the changes introduced by EGSnrc impacts the absorbed dose deposited in the air cavity of an ionization chamber. It is beyond the scope of this work to carry out a similar analysis of transmitted energy spectra.

4 Discussion

Using EGSnrc instead of EGS4 to calculate energy deposition spectra leads to energy shifts between the spectra that can be both positive and negative, but are always less than 17 keV in absolute value. By way of reference, the energy losses introduced by the various absorbers ranged from 150 keV to 3000 keV. The effect on the measured stopping powers reported in PIRS-0626 is larger for lower electron energies but is always less than 1 %.

The calculated EGSnrc and EGS4 spectra do not have the same shape and the differences are most noticeable for Ta absorbers where the reduced χ^2 is significantly greater than unity. Figure 10 compares the spectra for 15 MeV and a 3 g cm^{-2} Ta absorber. Relative to the EGS4 spectrum, EGSnrc predicts less energy deposition at high energy and more at lower energy, owing mostly for the inclusion of spin effects in the case of Ta, as shown. This implies that fewer high energy electrons are reaching the detector. If one were to normalize the spectra at the peak, the difference near 2 MeV is about 17 %. It may be that the statistical uncertainty of the measured spectra is adequate to test this difference. The remaining difference between the spectra in Figure 10 is due to core improvements in EGSnrc, notably its accurate multiple-scattering and boundary crossing algorithms.

Electron electronic stopping powers for several materials play an important role in radiation dosimetry. Water is often the reference material for radiation therapy dosimetry while air-filled ionization chambers are used as reference dosimeters. Absorbed dose calorimeters and ionization chambers are often constructed of graphite. Air-equivalent (C-552) or tissue-equivalent (A-150) plastics are sometimes used for ionization chamber walls.

The average energy to create an ion pair in air, W_{air}, is also an important quantity for dosimetry protocols and air kerma standards. Some of the most accurate values of W_{air} are obtained by comparing the absorbed dose measured calorimetrically to the absorbed dose measured using an ionization chamber in the same phantom material. Recent work has focused on determining the energy dependence of W_{air} over the energy range of importance to radiation dosimetry. Both graphite[18,19] and aluminum[20] have been used as the phantom material. The value obtained for W_{air} is inversely proportional to the stopping power of the calorimetric material.

The stopping power data reported in PIRS-0626 and refined here cover all of the materials mentioned above, except for air. Values are also given for Be, Cu and Ta. The key findings are as follows:

- The crystalline density should be used when evaluating the density effect correction for graphite. For 20 MeV electrons, this amounts to a 1 % difference compared to the value obtained if the bulk density is used.
- For water, C-552 and A-150, the measured and tabulated stopping powers are consistent.
- The measured values for aluminum are larger than the values tabulated in ICRU Report 37. Additional details are given in the following paragraph.
- For Be, Cu and Ta, which are typically not used for dosimetric purposes, the measured and tabulated stopping powers are consistent.

We now consider the impact of the graphite and aluminum stopping powers on recent efforts to measure W_{air}. Note that ICRU Report 90 has revised values for the stopping power of graphite but not for aluminum.

Values of the electronic stopping power as reported in PIRS-0626 but adjusted for the effect of using EGSnrc rather than EGS4, are shown in Figure 11. We note that the measured values for the graphite stopping power are in agreement with the values tabulated in ICRU Report 90, but the measured values for aluminum are larger. Quantitatively, the mean values and statistical standard uncertainties of the ratios are 0.07 ± 0.07 % and 0.57 ± 0.06 % for graphite and aluminum, respectively. According to PIRS-0626, the main systematic uncertainties arise from establishing the energy calibration of the detector system and measuring the thickness of the absorber slabs. The energy calibration is common to both graphite and aluminum so will not affect the difference between the two materials. The uncertainty of the slab thicknesses is stated to be "less than 0.2 %". Given that measurements with different slab thicknesses show consistency, it may be reasonable to assign an uncertainty of 0.15 % to both materials. Assuming no other systematic errors, the value of W_{air} determined using an aluminum phantom will be about 0.6 ± 0.2 % larger than the value obtained using a graphite phantom, if ICRU values are used for the stopping power.

5 Conclusions

Stopping powers are important for radiation dosimetry but there are no precision measurements for MeV electrons. PIRS-0626 reports measured values for the electronic stopping power from 5 to 30 MeV with an uncertainty of about 0.5 %, similar to the uncertainty of the best semi-empirical model. However, the data analysis used in that report was based on the EGS4 code rather than the more accurate EGSnrc code. We report corrections that can be applied to all the stopping power data in PIRS-0626.

The correction is larger for smaller energies but is always less than 1 %. For electron energies above 15 MeV the correction is generally less than 0.2 % and the conclusions of PIRS-0626 remain unchanged. For graphite, which is often used for dosimetric purposes, the effect is always less than 0.25 %, assuming the crystalline density is used to evaluate the density effect. PIRS-0626 reported only limited data for water but the correction is less than 0.2 %.

The fact that the differences due to using EGSnrc rather than EGS4 are small help to demonstrate that the technique proposed in PIRS-0626 is not strongly model-dependent. As reported in PIRS-0626, the largest discrepancy between the measured and tabulated stopping powers is for aluminum, and the present work does not change that fact. We show that this difference may become observable with recent work using aluminum phantoms to measure W_{air}.

Conflict of interest

The authors declare that they do not have any conflict of interest.

References

1. ICRU. Key Data for Ionizing-Radiation Dosimetry: Measurement Standards and Applications. ICRU Report 90. Bethesda, MD: International Commission on Radiation Units and Measurements, 2014.
2. IAEA. Absorbed dose determination in photon and electron beams: An international code of practice. Technical Report 277. Vienna: IAEA, 1987.
3. IAEA. Absorbed dose determination in external beam radiotherapy: An international code of practice for dosimetry based on standards of absorbed dose to water. Technical Report TRS-398. Vienna: IAEA, 2000.
4. Kawrakow I, Mainegra-Hing E, Rogers D, Tessier F, and Walters B. EGSnrc toolkit for Monte Carlo simulation of ionizing radiation transport. NRC Report PIRS-701. National Research Council Canada, 2015. DOI: 10.4224/40001303.
5. Salvat F. The PENELOPE code system. Specific features and recent improvements. Ann Nucl Energy 2015;82:98–109.
6. ICRU. Stopping powers for electrons and positrons. ICRU Report 37. Bethesda, MD: International Commission on Radiation Units and Measurements, 1984.
7. Faddegon BA, Ross CK, and Rogers DWO. Measurement of collision stopping powers of graphite, aluminium and copper for 10 and 20 MeV electrons. Phys Med Biol 1992;37:1561–71.

8. MacPherson M. Accurate measurements of the collision stopping powers for 5 to 30 MeV electrons. NRC Report PIRS-0626. Ottawa, Canada: National Research Council, 1998. DOI: 10.4224/40000364.

9. Roy T, Tessier F, and McEwen M. A system for the measurement of electron stopping powers: proof of principle using a pure β-emitting source. Rad Phys Chem 2018;149:134–41.

10. Nelson WR, Hirayama H, and Rogers DWO. The EGS4 Code System. SLAC Report 265. Stanford, California: Stanford University, 1985.

11. ICRU. Radiation dosimetry: Electron beams with energies between 1 and 50 MeV. ICRU Report 35. Bethesda, MD: International Commission on Radiation Units and Measurements, 1984.

12. Kawrakow I. Accurate condensed history Monte Carlo simulation of electron transport. I. EGSnrc, the new EGS4 version. Med Phys 2000;27:485–98.

13. Kawrakow I. Cross section improvements for EGSnrc. In: *Proceedings of the 22nd Annual International Conference of the IEEE Engineering in Medicine and Biology Society*. Vol. 3. 2000:1668–71. DOI: 10.1109/IEMBS.2000.900399.

14. Rogers DWO, Kawrakow I, Seuntjens JP, Walters BRB, and Mainegra-Hing E. NRC User Codes for EGSnrc. NRC Report PIRS-702. Ottawa: National Research Council, 2020. URL: https://nrc-cnrc.github.io/EGSnrc/doc/pirs702-egsnrc-codes.pdf.

15. RStudio Team. RStudio: Integrated Development Environment for R. RStudio, Inc. Boston, MA, 2015. URL: http://www.rstudio.com/.

16. Bevington PR and Robinson DK. Data reduction and error analysis for the physical sciences. Second Edition. New York: McGraw-Hill, 1992.

17. Kawrakow I. Accurate condensed history Monte Carlo simulation of electron transport. II. Application to ion chamber response simulations. Med Phys 2000;27:499–513.

18. Tessier F, Cojocaru CD, and Ross CK. Extracting W_{air} from the electron beam measurements of Domen and Lamperti. Med Phys 2018;45:370–81.

19. Bourgouin A, Cojocaru C, Ross C, and McEwen M. Determination of W_{air} in high-energy electron beams using graphite detectors. Med Phys 2019;46:5195–208.

20. Bourgouin A and McEwen M. Determination of W_{air} in high-energy clinical electron beams using aluminium detectors. In: *International Symposium on Standards, Applications and Quality Assurance in Medical Radiation Dosimetry*. IAEA, Vienna, 2019:31–2.

Supplementary Material

The following supporting information may be found online in the Supplementary Material associated to this article:

1. As a consistency check to test that our high-precision EGS4 spectra were equivalent to those calculated in 1997, we fitted one to the other to extract the energy shift. The results for all the spectra are shown in Figure S-1 and Figure S-2;

2. A sample EGSnrc input file `dosrz-10al10.egsinp` is provided for the case of 10 MeV electrons incident on an aluminum absorber with a mass thickness of 0.819 gm/cm^2, for anyone interested in reproducing the results with EGSnrc or investigating this topic further.

List of Figures

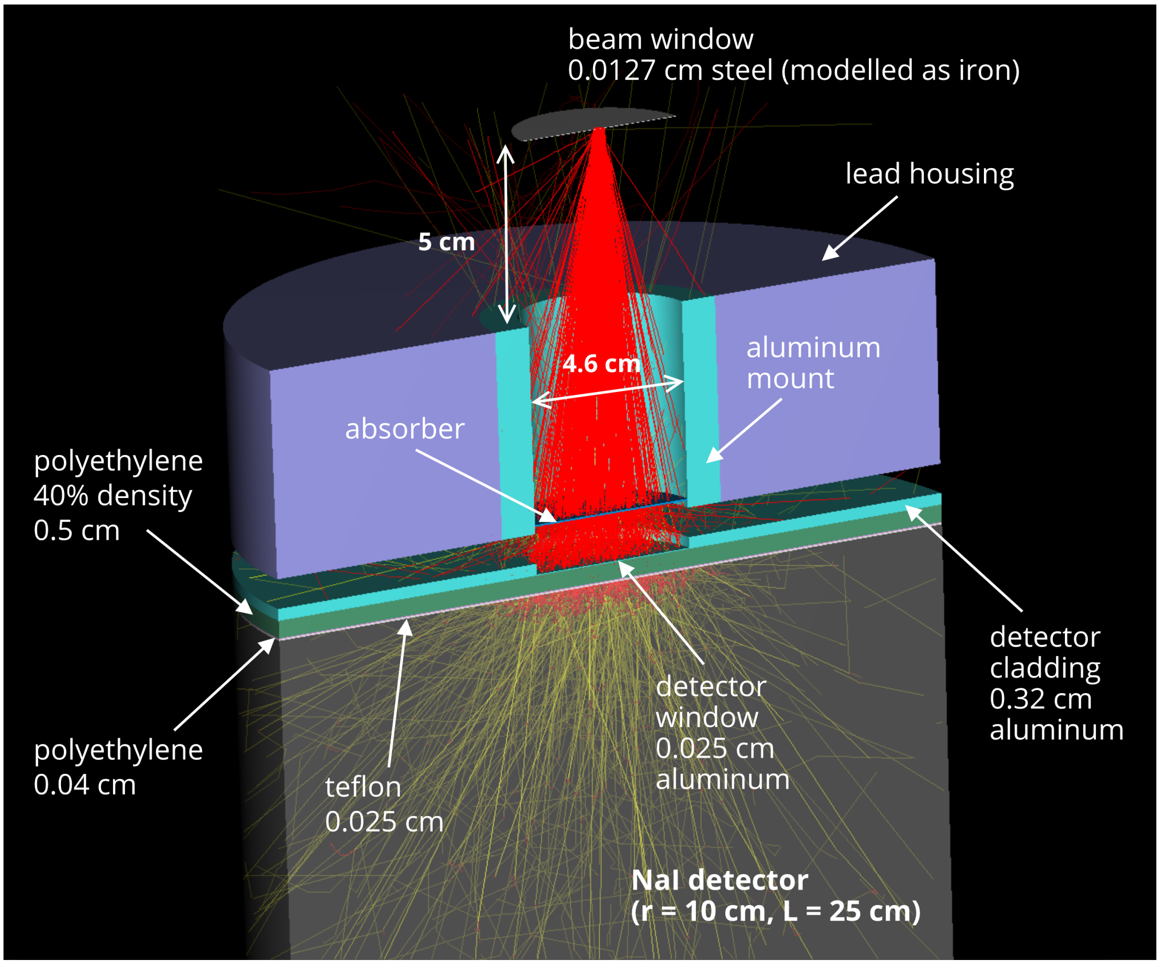

FIGURE 1 EGSnrc model of the detector used to measure electron stopping powers. A downward-directed pencil beam of electrons passed through the beam window of the accelerator and impinged on the absorber. The large NaI detector was used to measure the electron spectrum. Consult PIRS 0626[8] for more detail on the detector. In this image, the incident electron energy is 10 MeV and the absorber is tantalum (1 g/cm^2), and a few particle tracks are shown (electrons in red, photons in yellow).

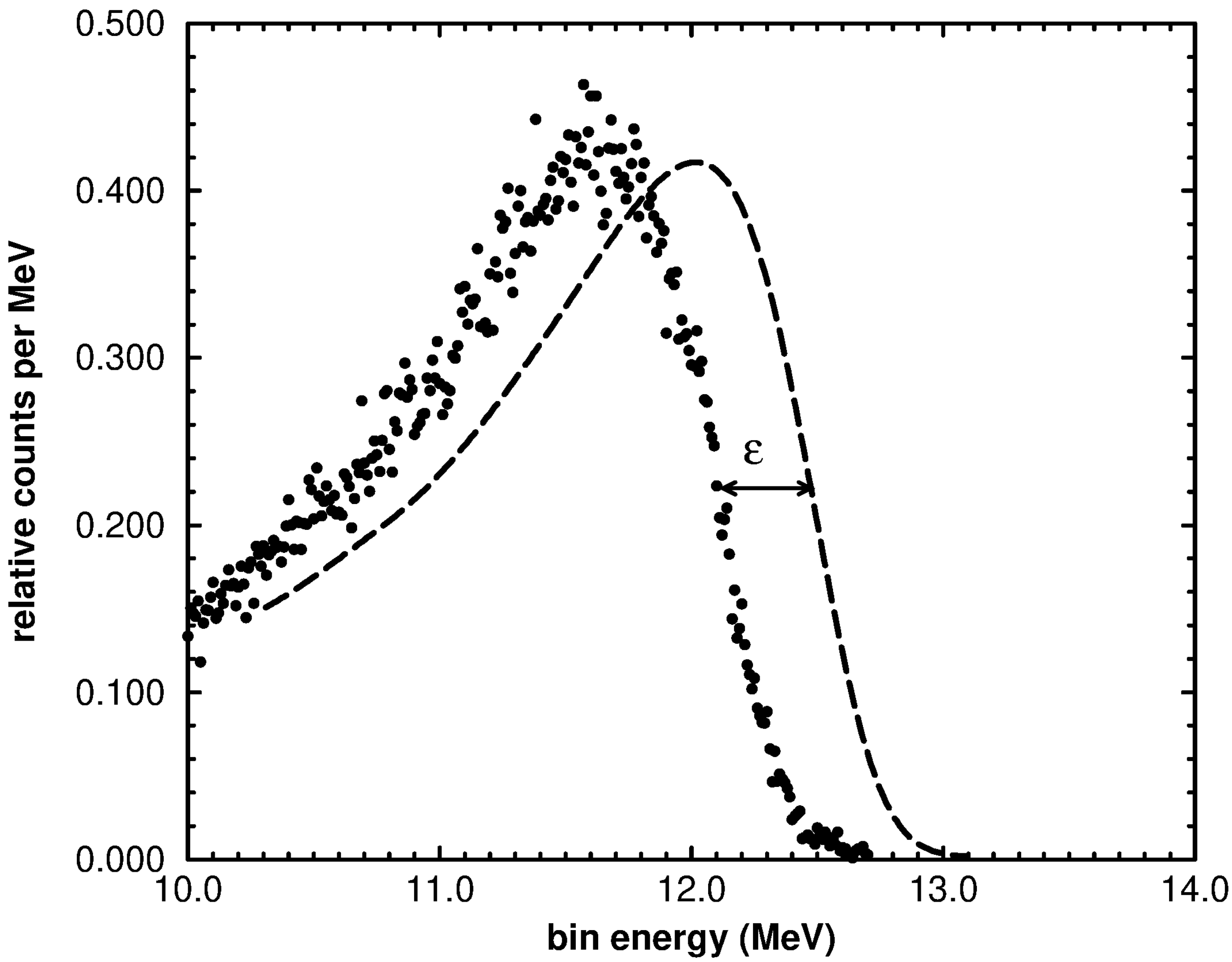

FIGURE 2 Typical spectrum (dots) measured with a 15 MeV electron beam and an Al absorber, 2 g cm^{-2} thick. The dashed line shows what the calculated MC spectrum might look like, although the offset has been exaggerated to illustrate the principle. Figure taken from PIRS 0626[8].

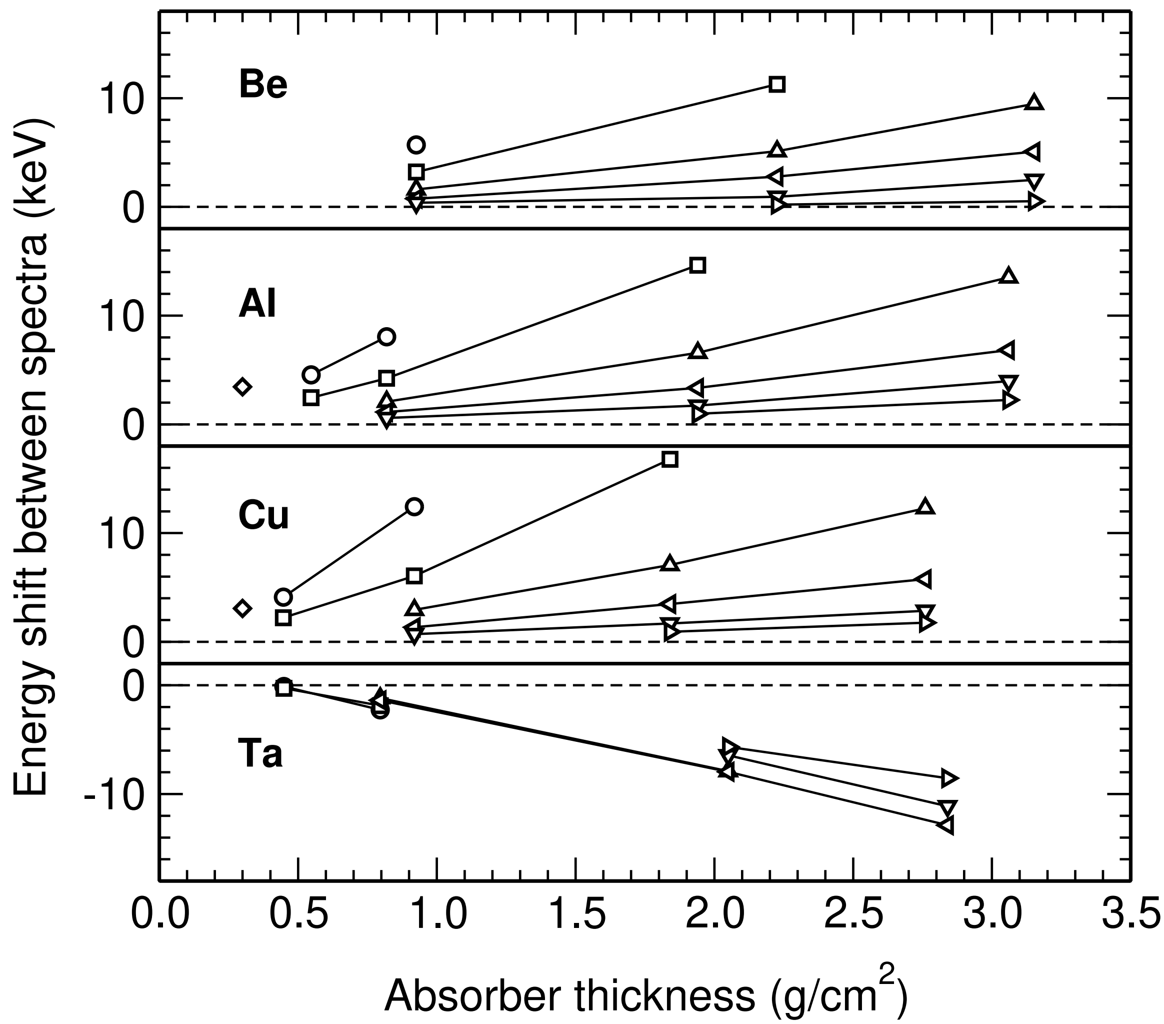

FIGURE 3 Energy shifts between the high-precision spectra calculated using EGS4 and EGSnrc. A positive value means that the EGSnrc spectrum is shifted to higher energy. These results are for the elemental materials Be, Al, Cu and Ta. The statistical uncertainty of each datum is typically smaller than the symbol size. The symbols identify the primary beam energy, as: ◇ 5 MeV; ○ 7 MeV; □ 10 MeV; △ 15 MeV; ◁ 20 MeV; ▽ 25 MeV; ▷ 30 MeV.

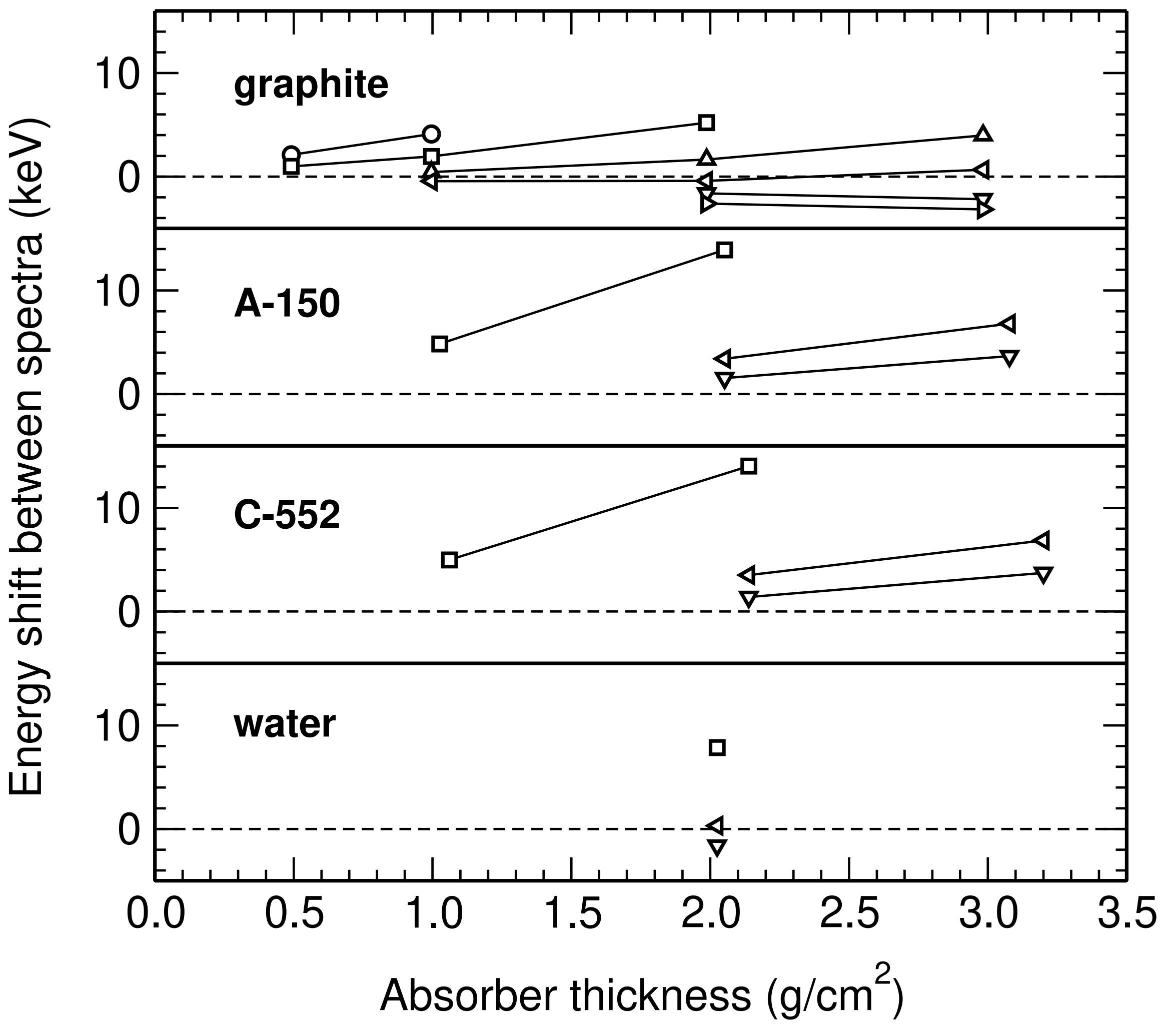

FIGURE 4 Same as Figure 3, but for materials that are often used for dosimetric purposes. PIRS-0626 reports results for only one absorber thickness of water.

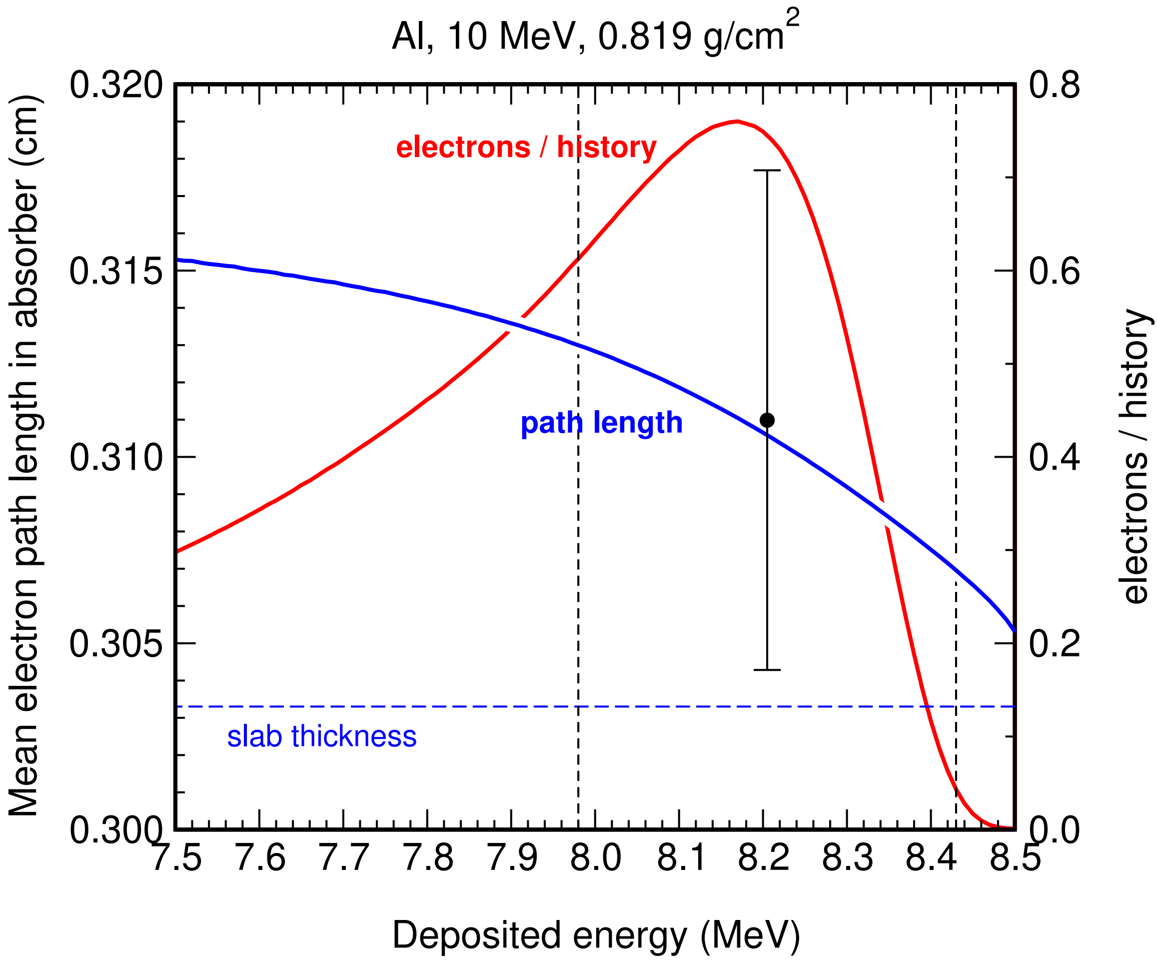

FIGURE 5 The mean path length (left axis, blue) and spectrum (right axis, red) of 10 MeV electrons passing through an aluminum slab 0.3033 cm thick, as a function of the energy deposited in the detector. The vertical dashed lines show the energy range used when fitting the spectra, and the horizontal dashed line indicates the physical slab thickness. The results were obtained from 1×10^9 histories and the uncertainty bars are smaller than the line width. The isolated data point gives the average path length over the fitting range (comprising about 2.5×10^8 path length samples), and the error bar represents the standard deviation of the path length distribution in that range (color online only).

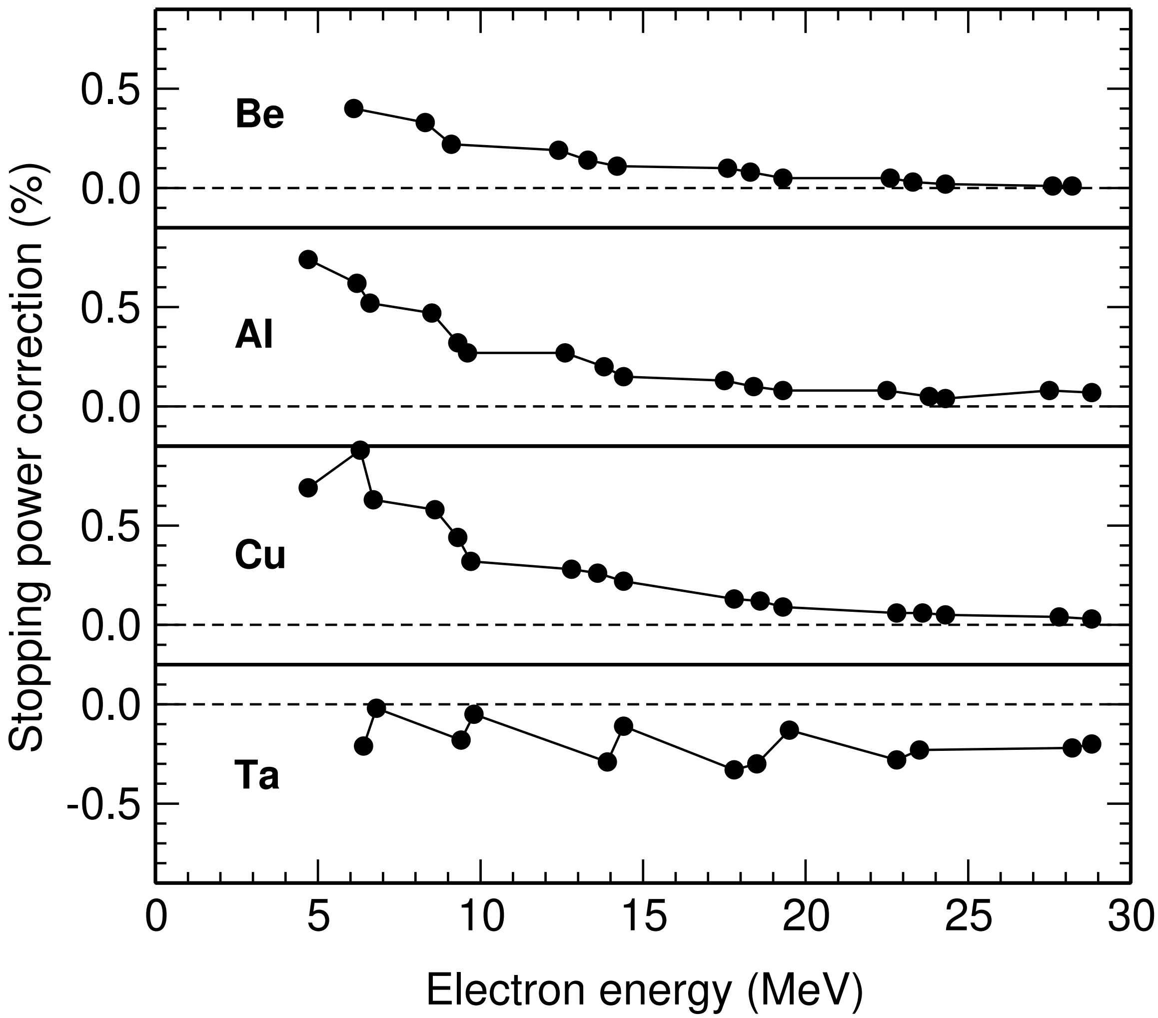

FIGURE 6 The percentage correction to the stopping power results presented in PIRS-0626 if EGSnrc is used instead of EGS4. The abscissa is the electron energy at the midpoint of the absorber and the values have been taken from PIRS-0626. These results are for the elemental materials Be, Al, Cu and Ta. The statistical uncertainty of each datum is typically smaller than the symbol size.

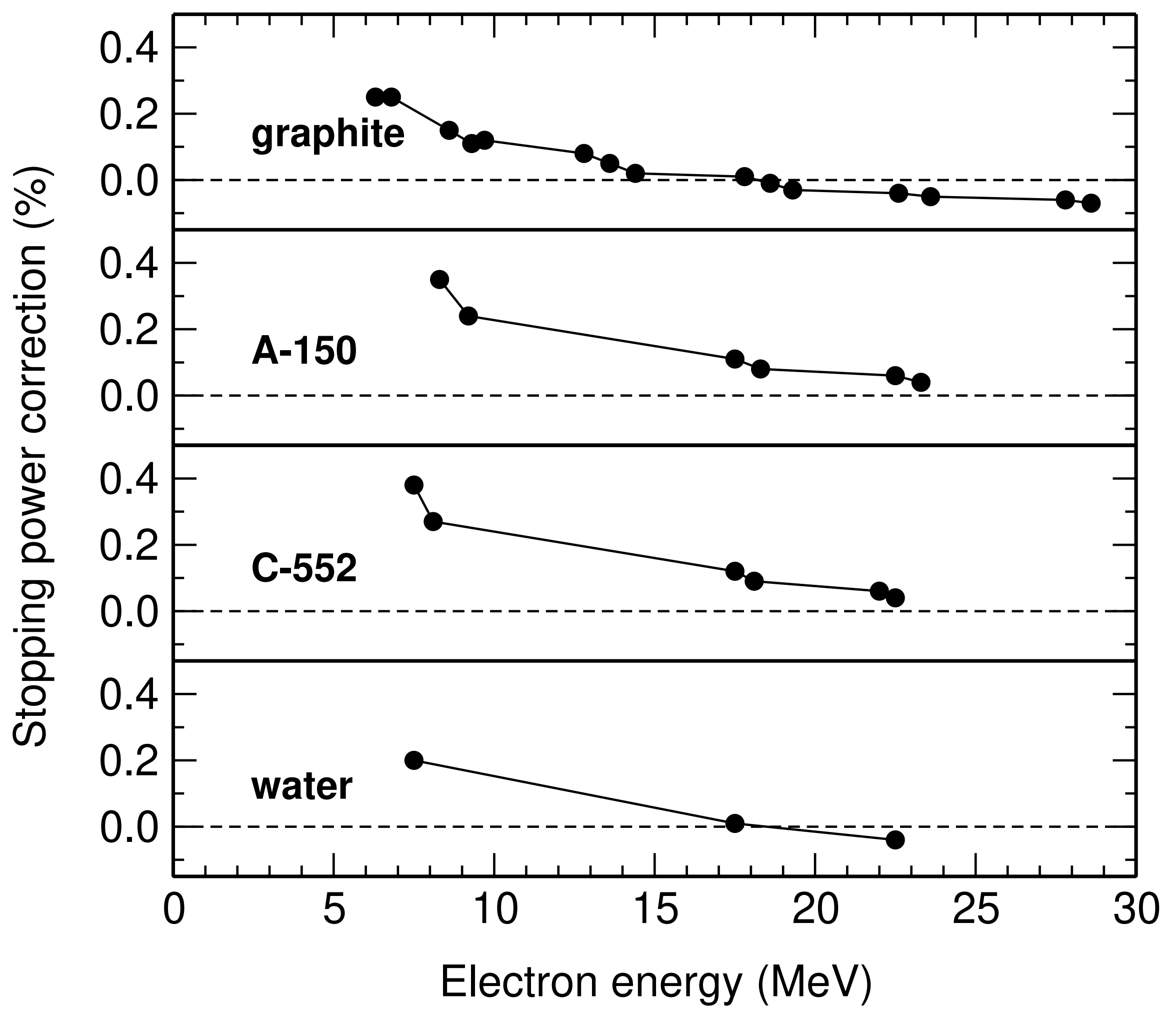

FIGURE 7 Same as Figure 6, but for materials that are often used for dosimetric purposes. PIRS-0626 reports results for only one absorber thickness of water.

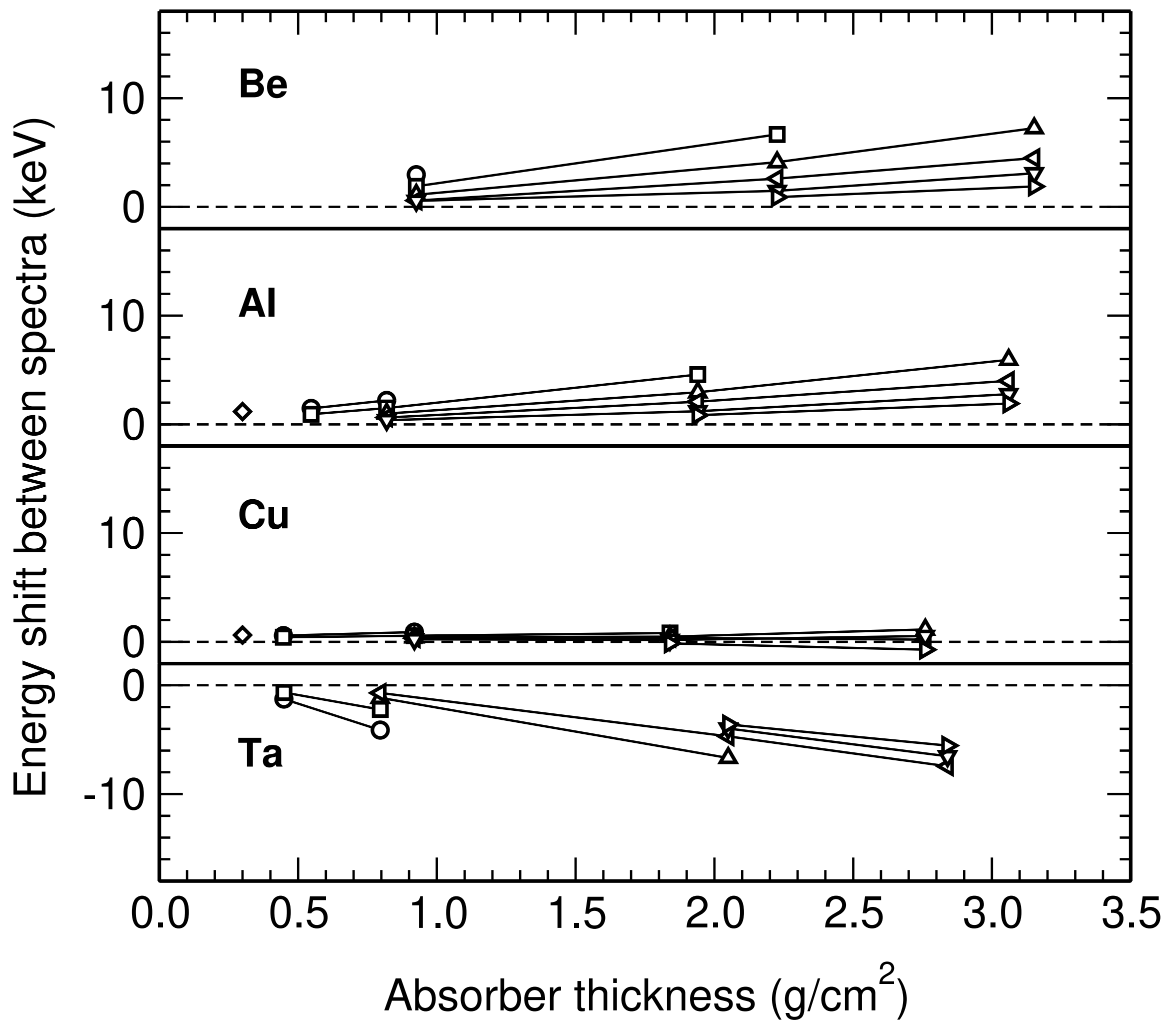

FIGURE 8 Energy shifts between spectra calculated using the full EGSnrc simulation and EGSnrc but with spin effects turned off. A positive value means that the full EGSnrc spectrum is shifted to higher energy. These results are for the elemental materials Be, Al, Cu and Ta. The statistical uncertainty of each datum is typically smaller than the symbol size. The symbols identify the primary beam energy, as: ◇ 5 MeV; ○ 7 MeV; □ 10 MeV; △ 15 MeV; ◁ 20 MeV; ▽ 25 MeV; ▷ 30 MeV.

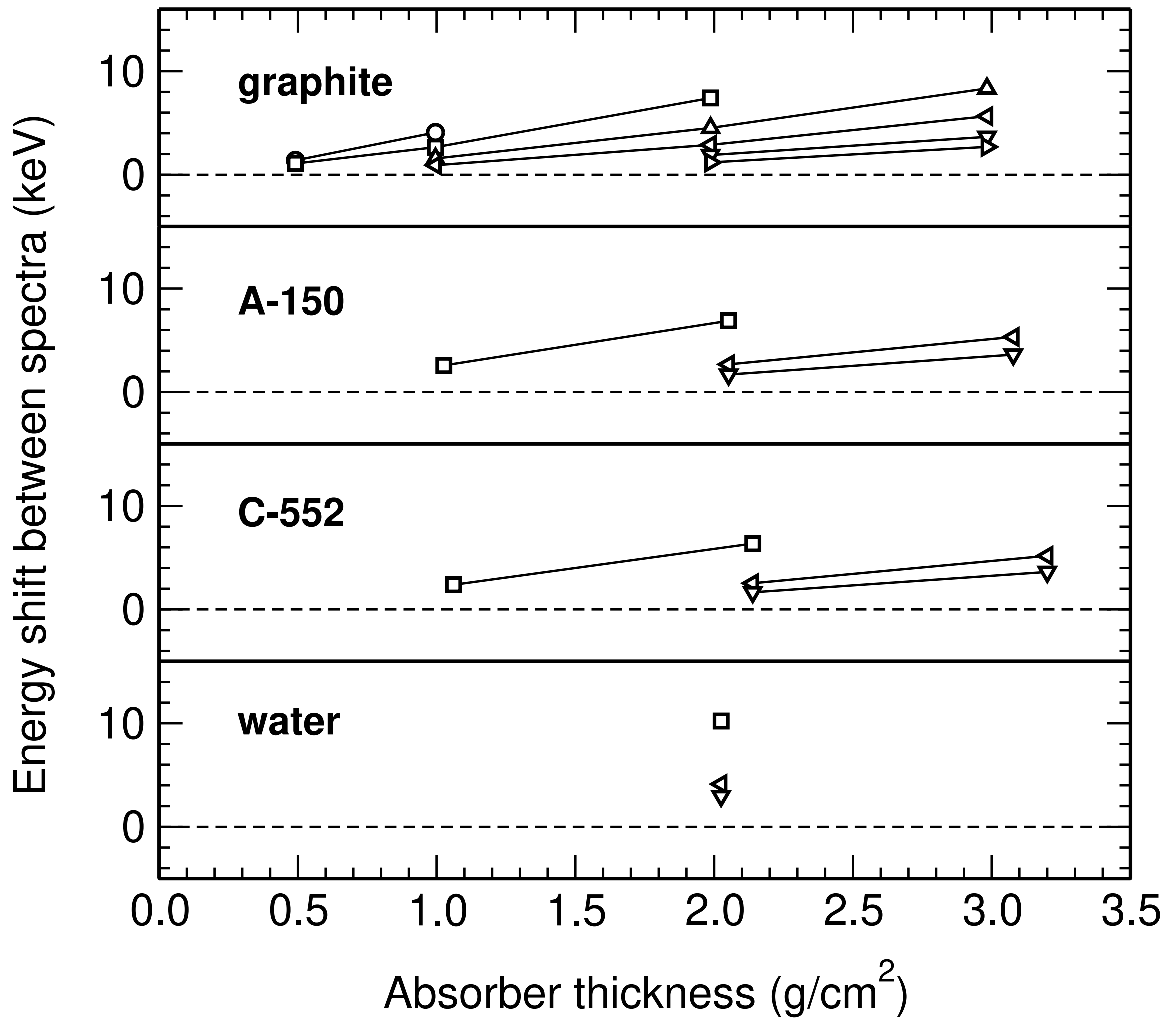

FIGURE 9 Same analysis as in Figure 8, but for materials that are often used for dosimetric purposes.

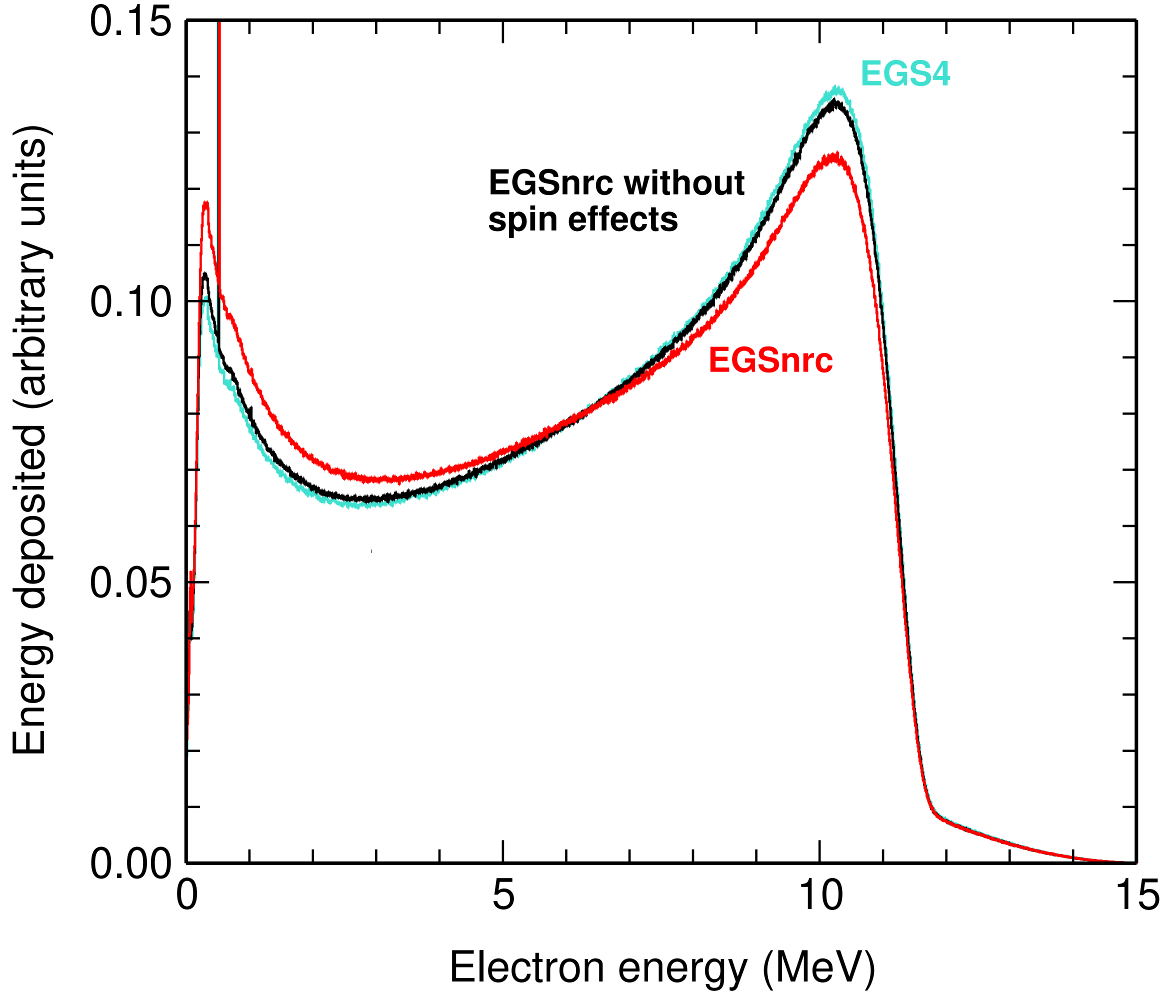

FIGURE 10 Comparison of the energy deposition spectra calculated with EGS4 (turquoise), EGSnrc (red) and EGSnrc without spin effects (black) for 15 MeV electrons incident on a 3 g cm^{-2} Ta absorber. Spectra are normalized so that the area under the curve is unity. The spectra have been calculated using 10 keV energy bins and the errors bars are shown but barely resolved at this scale. The sharp peak at 0.511 MeV is due to positron annihilation (color online only).

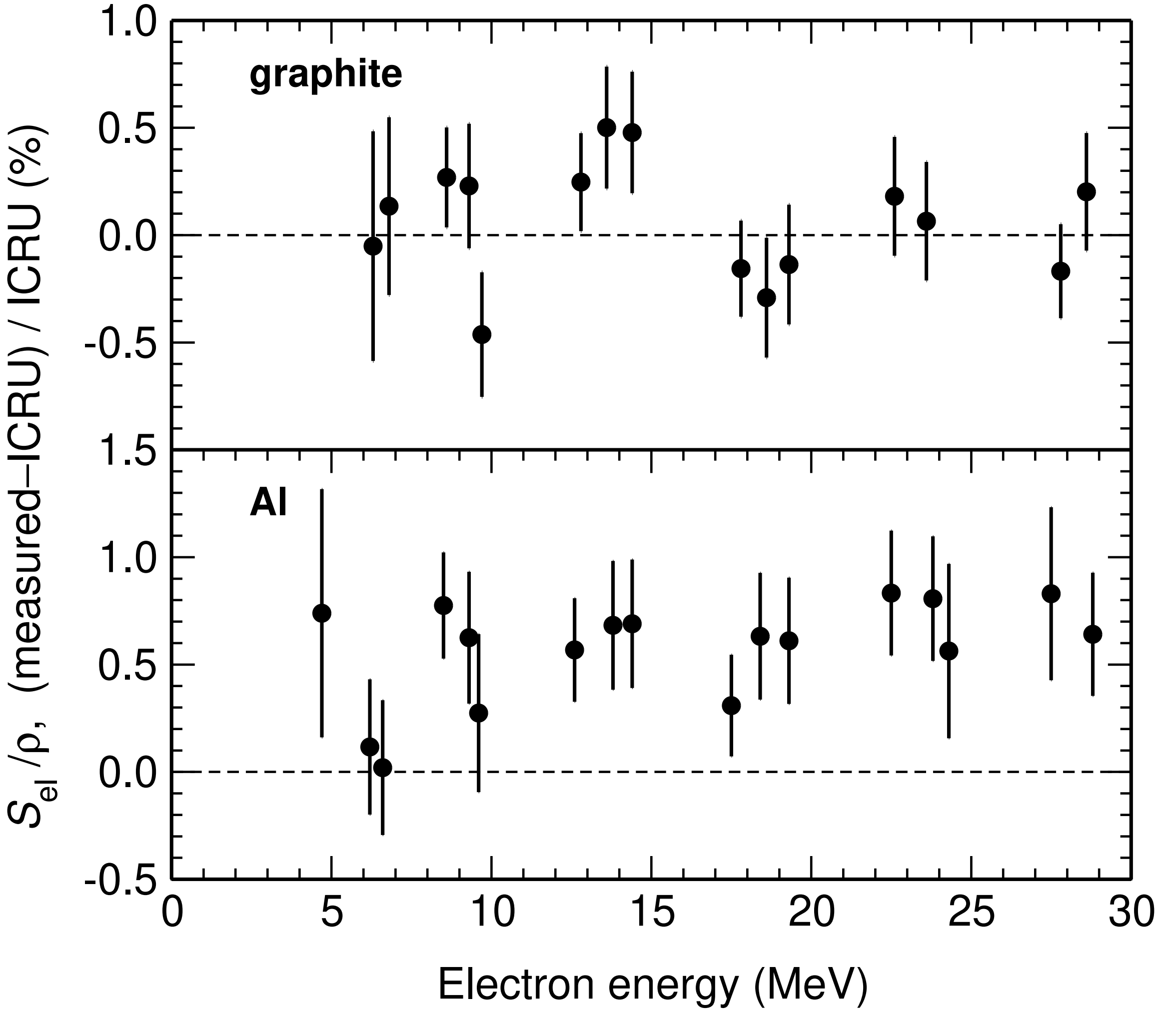

FIGURE 11 Corrected values of the electronic stopping power for graphite and aluminum. The results are presented as the percentage difference between the measured results and the values tabulated in ICRU 90 for graphite and in ICRU 37 for aluminum. The uncertainties are taken from PIRS-0626 as the contribution from comparing the spectra calculated with EGSnrc and EGS4 is negligible.

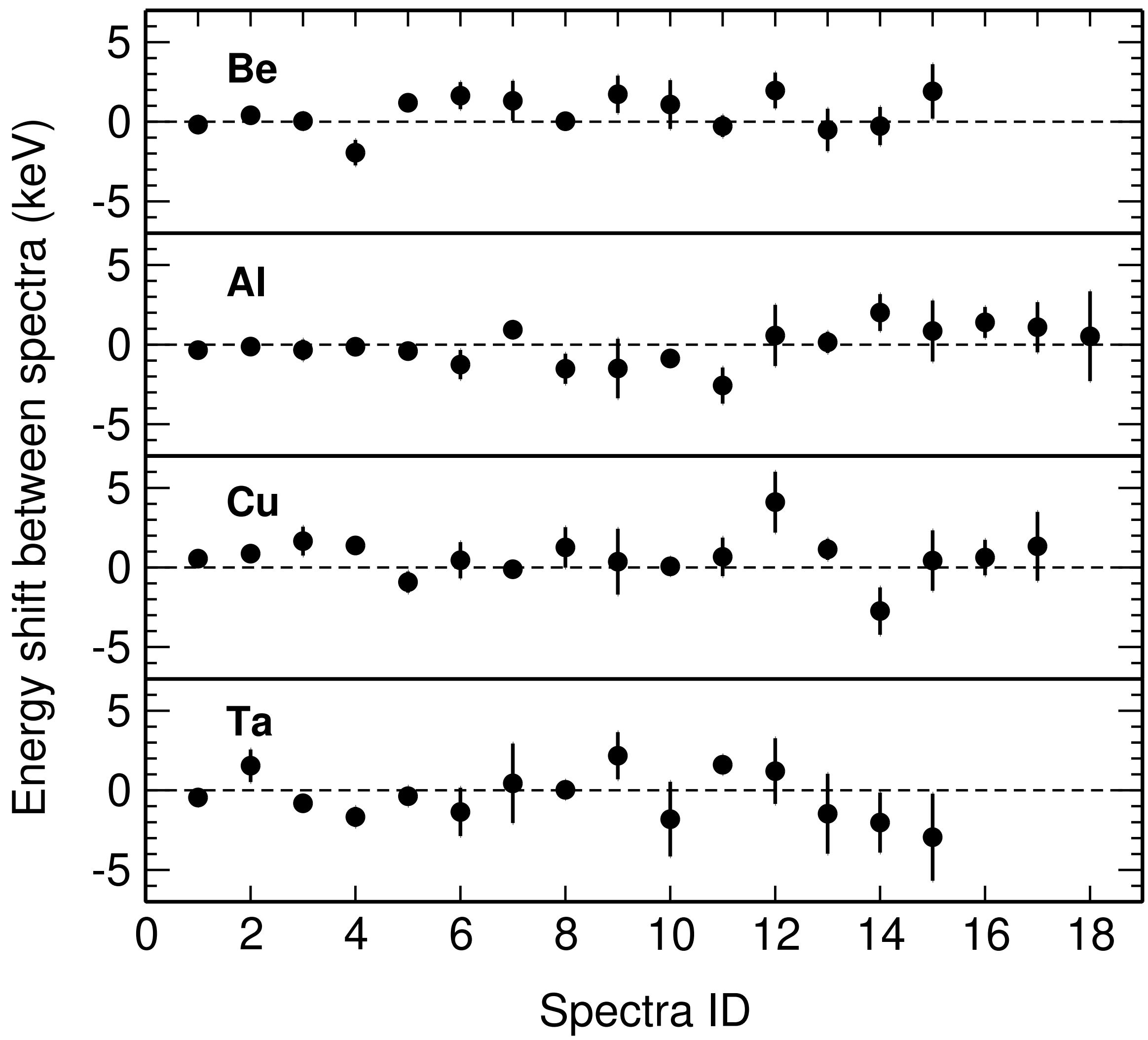

FIGURE S-1 Energy shifts between the original spectra used for extracting the stopping power data reported in PIRS-0626 and high-precision spectra calculated using EGS4. These results are for the elemental materials Be, Al, Cu and Ta. The abscissa is simply a number to identify each spectrum, but the low and high energy spectra are to the left and right, respectively.

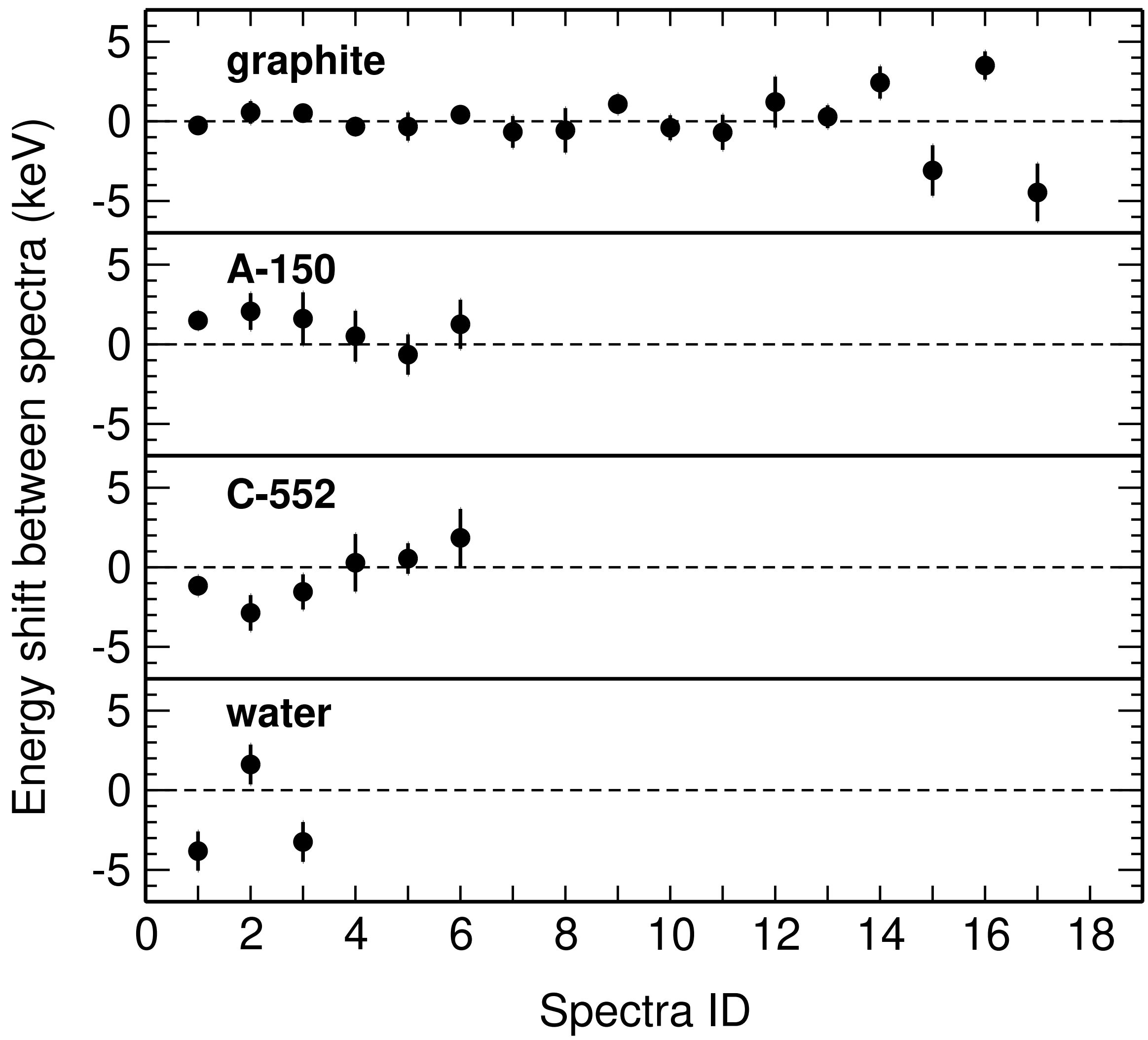

FIGURE S-2 Same as Figure S-1, but for materials that are often used for dosimetric purposes. Note that the graphite stopping power was calculated using the crystalline density to evaluate the density effect correction.

List of Tables

TABLE 1 Survey results for the electron path length over the energy range used for spectral fitting. The nominal mass thicknesses of the slabs are given in the first column, while the true linear thickness is given in the second. The fourth column gives the standard deviation of the path length distribution, σ_{tpl}, expressed as a fraction of the path length. The final column gives the approximate number of MC steps taken in transporting the electrons through the slab. The standard uncertainty on $t_{\mathrm{pl}}/t_{\mathrm{slab}}$ is of the order of 10^{-6}.

absorber	energy (MeV)	mass (g/cm^2)	t_{slab} (cm)	$t_{\mathrm{pl}}/t_{\mathrm{slab}}$	$\sigma_{\mathrm{tpl}}/t_{\mathrm{pl}}$	MC steps
Al	10	0.819	0.3033	1.025	0.022	23
Ta	7	0.798	0.0479	1.142	0.149	110
Al	30	3.058	1.133	1.015	0.017	42
Ta	30	2.841	0.1706	1.056	0.068	365